PROCEEDINGS OF SCIENCE

System-size dependence of particle production at mid- and forward rapidity with ALICE

Abhi Modak[a,*] **for the ALICE Collaboration**

[a] *Bose Institute,*
EN 80, Sector V, Bidhan Nagar, Kolkata, India

E-mail: abmodak@cern.ch

The pseudorapidity densities of charged particles and inclusive photons produced in high energy nuclear collisions are essential observables to characterise the global properties of the collisions, such as the achieved energy density, and to provide important constraints for Monte Carlo model calculations. In the LHC Run 1 and Run 2 configurations, ALICE had large coverage to measure charged particles over the pseudorapidity range $-3.4 < \eta < 5.0$, combining the data from the Silicon Pixel Detector (SPD) and the Forward Multiplicity Detector (FMD). The inclusive photons are measured at forward rapidity using the Photon Multiplicity Detector (PMD), covering the pseudorapidity range $2.3 < \eta < 3.9$. New results on charged-particle pseudorapidity densities measured in pp, p–Pb, and Pb–Pb collisions at $\sqrt{s_{\rm NN}}$ = 5.02 TeV using Run 1 and Run 2 data are presented. Inclusive photon production is reported for p–Pb collisions at $\sqrt{s_{\rm NN}}$ = 5.02 TeV. The charged-particle rapidity densities are derived from the measured charged-particle pseudorapidity densities, and then parameterized by a normal distribution. This allows us to study the evolution of the width of the rapidity distributions as a function of the number of participants in all three collision systems. The performance of the new Inner Tracking System (ITS) designed for ALICE Run 3 configuration is also discussed for pilot beam pp collisions at $\sqrt{s}$ = 0.9 TeV.

41st International Conference on High Energy physics - ICHEP2022
6-13 July, 2022
Bologna, Italy

*Speaker

PoS(ICHEP2022)461

1. Introduction

Particle production at the Large Hadron Collider (LHC) energies is driven by a combination of hard (perturbative) and soft (non-perturbative) quantum chromodynamics (QCD) processes. Soft QCD processes dominate the bulk of particle production at low transverse momenta and can only be described by phenomenological models and effective theories. Multiplicity and pseudorapidity distributions of the produced final-state particles are some of the basic measurements to characterise the global properties of the collisions [1] and to provide constraints for better tuning of models in understanding the underlying description of particle production. During the LHC Run 1 and Run 2, ALICE recorded data with various colliding systems (pp, p–Pb, Xe–Xe and Pb–Pb) at different center-of-mass energies. This offered the possibility to study the evolution of particle production with collision energy and system-size which will further help to learn about how the nuclear medium affects particle production mechanisms.

In this article, we report measurements of charged-particle pseudorapidity densities ($\mathrm{d}N_{\mathrm{ch}}/\mathrm{d}\eta$) in pp, p–Pb, and Pb–Pb collisions at mid- and forward rapidities using the ALICE detector [2]. The inclusive photon production, which provides the information complementary to those obtained from the charged particles, is studied in p–Pb collisions over the kinematic range $2.3 < \eta < 3.9$. The performance of the new Monolithic Active Pixel Sensors-based Inner Tracking System (ITS) (designed for ALICE Run 3 configuration [3]) and the tracking/matching algorithms are presented for LHC pilot run of pp collisions at $\sqrt{s} = 0.9$ TeV in October 2021.

2. Analysis method

The measurements of $\mathrm{d}N_{\mathrm{ch}}/\mathrm{d}\eta$ at $\sqrt{s_{\mathrm{NN}}} = 5.02$ TeV were performed based on the data collected by ALICE during LHC Run 1 for p–Pb collisions (in 2013) and during Run 2 for pp and Pb–Pb collisions (in 2015). The p–Pb and Pb–Pb data were analysed with a minimum bias (MB) trigger requiring a coincidence of signals in each side of the V0 sub-detectors (V0A and V0C). Likewise, the pp data were analysed for inelastic (INEL) interactions with at least one charged-particle detected at $|\eta| < 1$ (INEL > 0 event class). The standard ALICE event selection and centrality determination based on the V0 amplitude were considered in this analysis [4, 5]. The $\mathrm{d}N_{\mathrm{ch}}/\mathrm{d}\eta$ was measured by counting the number of tracklets using the SPD detector at mid-rapidity ($|\eta| < 2$). At forward rapidity the measurement was done based on the deposited energy signal in the FMD and a statistical method was employed to calculate the inclusive number of charged particles [4]. The detailed studies on the estimation of systematic uncertainties in pp, p–Pb and Pb–Pb collisions can be found in Ref. [4].

The $\mathrm{d}N_{\mathrm{ch}}/\mathrm{d}\eta$ was also analysed, using the new ALICE computing software framework, named Online-Offline (O^2) [6], for pp collisions at $\sqrt{s} = 0.9$ TeV using the pilot beam Run 3 data collected in October 2021. The events were selected using timing information of the Fast Interaction Trigger (FIT) detector [7]. The charged-particle tracks that have at least one hit in any of the ITS layers were considered in this analysis. Correction procedures similar to the ones described in [8] are used to correct the measured distributions. Systematic uncertainties from various sources (event generator dependence, p_{T} uncertainties, strangeness corrections and particle composition) were evaluated using techniques identical to those reported in [8].

The pseudorapidity density of inclusive photons ($\mathrm{d}N_\gamma/\mathrm{d}\eta$) was measured on an event-by-event basis using a preshower technique with the PMD detector [9–11]. The reconstruction of photons consists of two steps: (i) finding clusters of hits on the preshower plane of the PMD and (ii) discriminating between photons and charged hadrons. The clustering was performed using a nearest neighbour clustering algorithm. Each cluster is characterized by the number of cells (cluster N_{cell}) contained in it and the total energy (measured in terms of ADC) deposited in that cluster. Suitable photon-hadron discrimination thresholds were applied based on the cluster N_{cell} and ADC content to obtain a photon-rich sample, known as γ-like clusters [10]. A Bayesian unfolding technique [12] was then used to correct the measured distributions of γ-like clusters affected by instrumental effects and the contamination from hadron clusters [11]. A detailed discussion on the estimation of systematic uncertainties for the photon analysis is given in Refs. [10, 11].

3. Results and discussion

Figure 1 shows the primary charged-particle pseudorapidity densities measured in pp collisions with the INEL $>$ 0 event class and in top central (0–5%) p–Pb and Pb–Pb collisions at $\sqrt{s_{\mathrm{NN}}}$ = 5.02 TeV. The $\mathrm{d}N_{\mathrm{ch}}/\mathrm{d}\eta$ at mid-rapidity in pp collisions is found to be 5.7 ± 0.2 while for 0–5% Pb–Pb collisions it reaches ≈ 2000. A clear asymmetric shape of $\mathrm{d}N_{\mathrm{ch}}/\mathrm{d}\eta$ is observed in p–Pb collisions and the distribution peaks at $\mathrm{d}N_{\mathrm{ch}}/\mathrm{d}\eta \approx 60$ around $\eta = 3$ on the Pb-going direction.

The ratio of the charged-particle pseudorapidity density, $r_X = (\mathrm{d}N_{\mathrm{ch}}/\mathrm{d}\eta|_X)/(\mathrm{d}N_{\mathrm{ch}}/\mathrm{d}\eta)|_{\mathrm{pp}}$ (where X labels centrality classes in p–Pb and Pb–Pb collisions), in p–Pb and Pb–Pb collisions to that in pp collisions is presented as a function of η in Fig. 2a. It is observed that the ratio, r_{pPb}, increases linearly with η from the p-going to the Pb-going direction for central collisions which suggests a scaling of the pp distribution with the increasing number of participants as the lead nucleus is probed by the incident proton. A similar scaling, however, is not observed in the ratio of the Pb–Pb distributions relative to the pp. The r_{PbPb} exhibits an enhancement of particle production around $\eta = 0$ for the more central collisions.

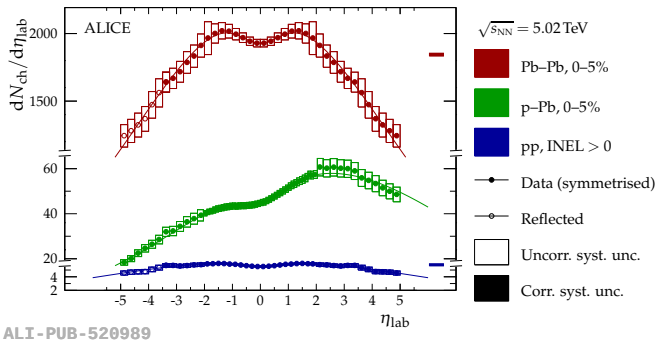

Figure 1: Charged-particle pseudorapidity density for minimum bias (INEL $>$ 0) pp and for the 5% most central p–Pb and Pb–Pb collisions at $\sqrt{s_{\mathrm{NN}}}$ = 5.02 TeV. The lines show fits of Eq. 1 (Pb–Pb and pp) and Eq. 2 (p–Pb) to the data (see text). Please note that the ordinate has been cut twice to accommodate for the very different ranges of the $\mathrm{d}N_{\mathrm{ch}}/\mathrm{d}\eta$ [4].

The charged-particle rapidity density ($\mathrm{d}N_{\mathrm{ch}}/\mathrm{d}y$) in Pb–Pb collisions [13], to a good accuracy, is observed to follow a normal distribution within $|y| \lesssim 5$. The conversion of $\mathrm{d}N_{\mathrm{ch}}/\mathrm{d}\eta$ to $\mathrm{d}N_{\mathrm{ch}}/\mathrm{d}y$ is given by $\mathrm{d}N_{\mathrm{ch}}/\mathrm{d}\eta = \left(1 + \frac{m^2}{p_{\mathrm{T}}^2 \cosh^2\eta}\right)^{-1/2} \mathrm{d}N_{\mathrm{ch}}/\mathrm{d}y$. Hence, $\mathrm{d}N_{\mathrm{ch}}/\mathrm{d}\eta$ for symmetric collision systems (pp and Pb–Pb) can be parameterized as [4, 13]

$$f(\eta; A, a, \sigma) = \left(1 + 1/a^2 \cosh^2\eta\right)^{-1/2} \left(A/\sqrt{2\pi}\sigma\right) \exp\left(-y^2(\eta, a)/2\sigma^2\right) \quad (1)$$

where $a = p_{\mathrm{T}}/m$, A and σ are the total integral and width of the distribution, respectively, and y the rapidity in the center-of-mass frame. Based on the observation of the linear increase of the p–Pb to pp ratios, the $\mathrm{d}N_{\mathrm{ch}}/\mathrm{d}\eta$ for the asymmetric system (p–Pb) can also be parameterized as

$$g(\eta; A, a, \beta, \sigma) = \left(1 + 1/a^2 \cosh^2 \eta\right)^{-1/2} \left[(\beta y(\eta, a) + A)/\sqrt{2\pi}\sigma\right] \exp\left(-[y(\eta, a) - y_{\mathrm{CM}}]^2/2\sigma^2\right) \quad (2)$$

where A is replaced by $(\beta y(\eta, a) + A)$ which is linear in y multiplied by a factor β. and $y_{\mathrm{CM}} = 0.465$ which is the rapidity of the center-of-mass system in the laboratory frame. Best-fit parameterizations of the measured $\mathrm{d}N_{\mathrm{ch}}/\mathrm{d}\eta$ in terms of Eq. 1 (for pp and Pb–Pb) and Eq. 2 (for p–Pb) are shown in Fig. 1. The charged-particle pseudorapidity distributions are well described by these two functions f and g, indicating that the particle production in pp, p–Pb, and Pb–Pb collisions follow a normal distribution in rapidity.

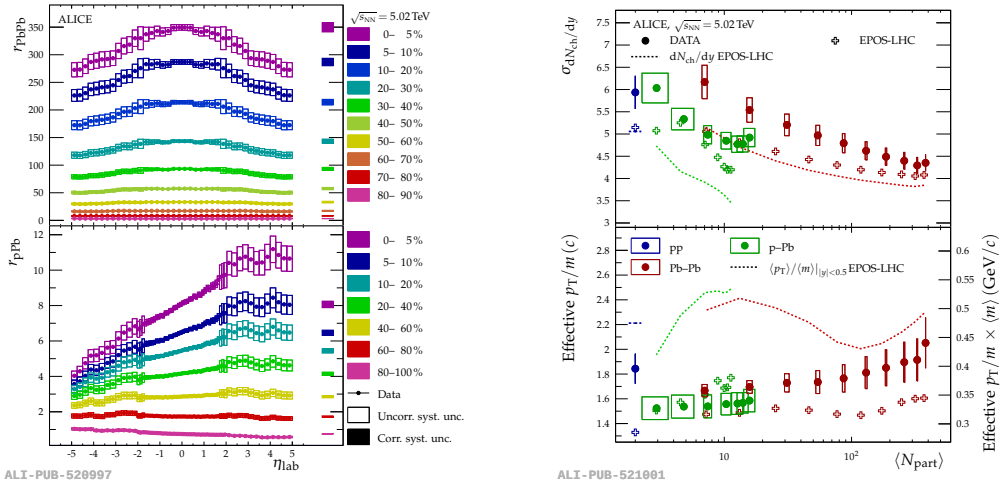

(a) **(b)**

Figure 2: (a) The ratio of the charged-particle pseudorapidity density measured in Pb–Pb (top) and p–Pb (bottom) in different centrality classes to the same quantity obtained in pp for the INEL > 0 event class. Note, for Pb–Pb η_{lab} is the same as the center-of-mass pseudorapidity. (b) The width (top) and effective p_{T}/m (bottom) extracted from best-fit parameterizations using Eq. 1 and Eq. 2 are shown as a function of mean number of participants. Similar fit parameters from the same parameterisation of EPOS-LHC calculations are also shown [4].

The top panel of Fig. 2b presents the width of the charged-particle rapidity distributions ($\sigma_{\mathrm{d}N_{\mathrm{ch}}/\mathrm{d}y}$) for pp, p–Pb, and Pb–Pb collisions as a function of the average number of participating nucleons ($\langle N_{\mathrm{part}} \rangle$) calculated using a Glauber model. The $\sigma_{\mathrm{d}N_{\mathrm{ch}}/\mathrm{d}y}$ extracted from the same parameterisation of the EPOS-LHC calculations [14] is shown by open markers. The dashed lines are obtained directly by evaluating the width of the charged particle rapidity density from EPOS-LHC model. The general trend is that the $\sigma_{\mathrm{d}N_{\mathrm{ch}}/\mathrm{d}y}$ decreases as $\langle N_{\mathrm{part}} \rangle$ increases, consistent with the behaviour of the Pb–Pb to pp ratios. It is also noted that the width of the $\mathrm{d}N_{\mathrm{ch}}/\mathrm{d}y$ distributions in p–Pb and Pb–Pb approaches that of the pp distribution at low $\langle N_{\mathrm{part}} \rangle$. These results suggest that the enhancement of particle production near mid-rapidity in Pb–Pb is an effect of the nuclear medium. The bottom panel of Fig. 2b shows the dependence of the parameter a on $\langle N_{\mathrm{part}} \rangle$. The right-hand ordinate is the same but multiplied by the average $\langle m \rangle = (0.215 \pm 0.001)$ GeV/c^2. The parameter a

extracted from the EPOS-LHC calculations [14] is also presented (open markers) in the figure. The dashed lines represent the average p_T/m predicted by the EPOS-LHC [14]. The model calculations indicate that the extracted transverse momentum to mass ratio a is smaller than the $\langle p_T \rangle / \langle m \rangle$.

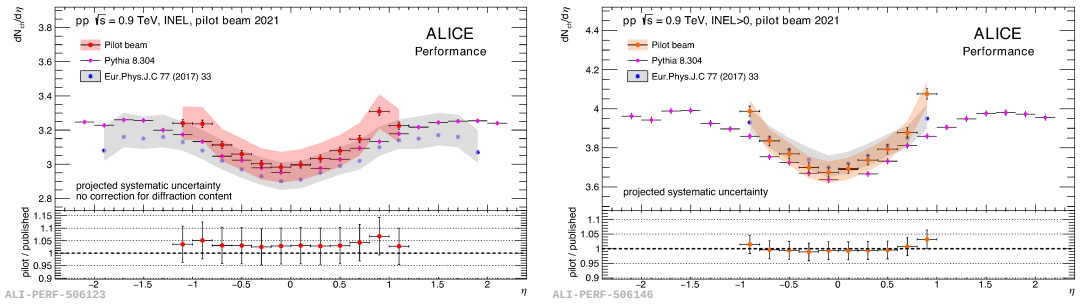

(a) **(b)**

Figure 3: Charged-particle pseudorapidity densities in pp collisions at $\sqrt{s}$ = 0.9 TeV for INEL (a) and INEL > 0 (b) event classes are presented together with ALICE's previous measurements [15] and PYTHIA [16] model predictions.

Figures 3a and 3b present the measurements of $\mathrm{d}N_{\mathrm{ch}}/\mathrm{d}\eta$ using Run 3 pilot beam data in pp collisions at $\sqrt{s}$ = 0.9 TeV for INEL and INEL > 0 event classes respectively. The results are compared to the published Run 2 measurements [15]. The difference between Run 2 and Run 3 measurements comes mainly from: (a) the upgraded ALICE detector and (b) new reconstruction algorithms. It is observed that there is good agreement between the present measurements and published results. However, the measurements for the INEL event class is slightly higher than the published data due to the lack of diffraction correction in the Run 3 Monte Carlo (MC) simulation. PYTHIA 8 [16] explains the data within uncertainties. These results validate the performance of the new ITS as well as the new reconstruction algorithms.

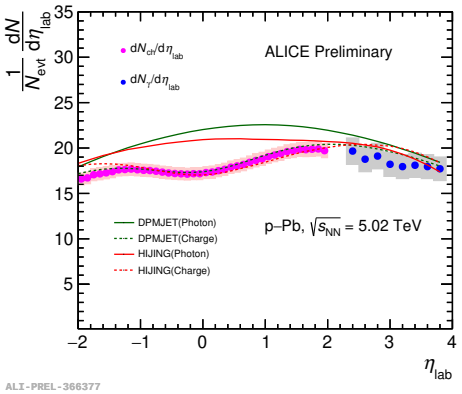

Figure 4: $\mathrm{d}N_\gamma/\mathrm{d}\eta$ measured in p–Pb collisions at $\sqrt{s_{\mathrm{NN}}}$ = 5.02 TeV for MB events. The results are compared with similar measurements for charged particles at mid-rapidity [17]. Predictions from HIJING [18] and DPMJET [19] are superimposed.

Figure 4 presents the $\mathrm{d}N_\gamma/\mathrm{d}\eta$ (solid blue circles) measured for MB events in p–Pb collisions at $\sqrt{s_{\mathrm{NN}}}$ = 5.02 TeV in the pseudorapidity interval $2.3 < \eta < 3.9$, together with the measurements of charged-particle production (solid magenta circles) at mid-rapidity [17]. The measurements are compared with the predictions from HIJING [18] and DPMJET [19] event generators. Both MC models considered here are in good agreement with $\mathrm{d}N_{\mathrm{ch}}/\mathrm{d}\eta$ whereas $\mathrm{d}N_\gamma/\mathrm{d}\eta$ is slightly overpredicted by DPMJET. These results provide new constraints on model calculations to understand particle, and in particular photon, production in p–Pb collisions.

4. Summary

We have presented and compared the charged-particle pseudorapidity density measured in pp, p–Pb, and Pb–Pb collisions at $\sqrt{s_{\rm NN}}$ = 5.02 TeV. A clear enhancement of particle production at mid-rapidity in central Pb–Pb collisions compared to pp collisions is observed whereas a linear scaling is seen for p–Pb collisions with respect to the pp collisions. By transforming the pseudorapidity distributions to rapidity distributions we have found that the measurements for all three collision systems follow a normal distribution in rapidity. We have analysed the pilot beam data in pp collisions at $\sqrt{s}$ = 0.9 TeV using the new ITS detector and the brand new computing framework and the performance of the whole setup has been studied, obtaining excellent perspective in view of Run 3 data taking. Finally, we have also measured the $\mathrm{d}N_\gamma/\mathrm{d}\eta$ at forward rapidity which follows the trend of charged-particle measurements at mid-rapidity.

References

[1] J. D. Bjorken, Phys. Rev. D **27** (1983), 140-151.

[2] B. B. Abelev *et al.* [ALICE Collaboration], Int. J. Mod. Phys. A **29**, 1430044 (2014).

[3] B. Abelev *et al.* [ALICE Collaboration], J. Phys. G **41** (2014), 087001.

[4] C. H. Christensen *et al.* [ALICE Collaboration], [arXiv:2204.10210 [nucl-ex]].

[5] B. Abelev *et al.* [ALICE Collaboration], Phys. Rev. C **88** (2013) no.4, 044909, [arXiv:1301.4361 [nucl-ex]].

[6] A. Alkin *et al.* EPJ Web Conf. **251**, 03063 (2021).

[7] W. H. Trzaska [ALICE Collaboration], Nucl. Instrum. Meth. A **845**, 463-466 (2017).

[8] J. Adam *et al.* [ALICE Collaboration], Eur. Phys. J. C **77**, no.1, 33 (2017), [arXiv:1509.07541 [nucl-ex]].

[9] M. M. Aggarwal *et al.*, Nucl. Instrum. Meth. A **488**, 131-143 (2002) [arXiv:nucl-ex/0112016 [nucl-ex]].

[10] B. B. Abelev *et al.*, [ALICE Collaboration], Eur. Phys. J. C **75**, no.4, 146 (2015).

[11] A. Modak [ALICE Collaboration], PoS **LHCP2021** (2021), 217, [arXiv:2110.05157 [hep-ex]].

[12] G. D'Agostini, Nucl. Instrum. Meth. A **362**, 487-498 (1995).

[13] J. Adam *et al.* [ALICE Collaboration], Phys. Lett. B **772**, 567-577 (2017), [arXiv:1612.08966 [nucl-ex]].

[14] T. Pierog *et al.* Phys. Rev. C **92**, no.3, 034906 (2015) [arXiv:1306.0121 [hep-ph]].

[15] J. Adam *et al.* [ALICE Collaboration], Eur. Phys. J. C **77**, no.1, 33 (2017) [arXiv:1509.07541 [nucl-ex]].

[16] C. Bierlich *et al.* [arXiv:2203.11601 [hep-ph]].

[17] B. Abelev *et al.* [ALICE Collaboration], Phys. Rev. Lett. **110**, no.3, 032301 (2013).

[18] X. N. Wang and M. Gyulassy, Phys. Rev. D **44**, 3501-3516 (1991).

[19] S. Roesler, R. Engel and J. Ranft, International Conference on Advanced Monte Carlo for Radiation Physics, Particle Transport Simulation and Applications (MC 2000), pp. 1033-1038. 12, 2000. [arXiv:hep-ph/0012252 [hep-ph]].